Eight-fold signal amplification of a superconducting nanowire single-photon detector using a multiple-avalanche architecture

Qingyuan Zhao,[1,2] Adam N. McCaughan,[2] Andrew E. Dane,[2] Faraz Najafi,[2] Francesco Bellei,[2] Domenico De Fazio,[2,3] Kristen A. Sunter,[2] Yachin Ivry,[2] and Karl K. Berggren[2,*]

[1]Research Institute of Superconductor Electronics (RISE), School of Electronic Science and Engineering, Nanjing University, Nanjing 210093, China
[2]Department of Electrical Engineering and Computer Science, Massachusetts Institute of Technology, 77 Massachusetts Avenue, Cambridge, Massachusetts 02139, USA
[3]Department of Electronics and Telecommunications (DET), Polytechnic University of Turin, Corso Duca Degli Abruzzi 24, Torino 10129, Italy
[*]berggren@mit.edu

Abstract: Superconducting nanowire avalanche single-photon detectors (SNAPs) with n parallel nanowires are advantageous over single-nanowire detectors because their output signal amplitude scales linearly with n. However, the SNAP architecture has not been viably demonstrated for $n > 4$. To increase n for larger signal amplification, we designed a multi-stage, successive-avalanche architecture which used nanowires, connected via choke inductors in a binary-tree layout. We demonstrated an avalanche detector with $n = 8$ parallel nanowires and achieved eight-fold signal amplification, with a timing jitter of 54 ps.

OCIS codes: (270.5570) Quantum detectors; (220.0220) Optical design and fabrication; (030.5260) Photon counting.

References and links

1. E. Knill, R. Laflamme, and G. J. Milburn, "A scheme for efficient quantum computation with linear optics," Nature **409**(6816), 46–52 (2001).
2. N. Gisin and R. Thew, "Quantum communication," Nat. Photonics **1**(3), 165–171 (2007).
3. R. H. Hadfield, "Single-photon detectors for optical quantum information applications," Nat. Photonics **3**(12), 696–705 (2009).
4. Q. Zhao, L. Zhang, T. Jia, L. Kang, W. Xu, J. Chen, and P. Wu, "Intrinsic timing jitter of superconducting nanowire single-photon detectors," Appl. Phys. B **104**(3), 673–678 (2011).
5. L. You, X. Yang, Y. He, W. Zhang, D. Liu, W. Zhang, L. Zhang, L. Zhang, X. Liu, S. Chen, Z. Wang, and X. Xie, "Jitter analysis of a superconducting nanowire single photon detector," AIP Adv. **3**(7), 072135 (2013).
6. A. Divochiy, F. Marsili, D. Bitauld, A. Gaggero, R. Leoni, F. Mattioli, A. Korneev, V. Seleznev, N. Kaurova, O. Minaeva, G. Gol'tsman, K. G. Lagoudakis, M. Benkhaoul, F. Lévy, and A. Fiore, "Superconducting nanowire photon-number-resolving detector at telecommunication wavelengths," Nat. Photonics **2**(5), 302–306 (2008).
7. S. Miki, T. Yamashita, Z. Wang, and H. Terai, "A 64-pixel NbTiN superconducting nanowire single-photon detector array for spatially resolved photon detection," Opt. Express **22**(7), 7811–7820 (2014).
8. S. Jahanmirinejad and A. Fiore, "Proposal for a superconducting photon number resolving detector with large dynamic range," Opt. Express **20**(5), 5017–5028 (2012).
9. Q. Zhao, A. McCaughan, F. Bellei, F. Najafi, D. De Fazio, A. Dane, Y. Ivry, and K. K. Berggren, "Superconducting-nanowire single-photon-detector linear array," Appl. Phys. Lett. **103**(14), 142602 (2013).
10. Z. Zhou, S. Jahanmirinejad, F. Mattioli, D. Sahin, G. Frucci, A. Gaggero, R. Leoni, and A. Fiore, "Superconducting series nanowire detector counting up to twelve photons," Opt. Express **22**(3), 3475–3489 (2014).
11. M. Ejrnaes, R. Cristiano, O. Quaranta, S. Pagano, A. Gaggero, F. Mattioli, R. Leoni, B. Voronov, and G. Gol'tsman, "A cascade switching superconducting single photon detector," Appl. Phys. Lett. **91**(26), 262509 (2007).
12. F. Marsili, F. Najafi, E. Dauler, F. Bellei, X. Hu, M. Csete, R. J. Molnar, and K. K. Berggren, "Single-photon detectors based on ultranarrow superconducting nanowires," Nano Lett. **11**(5), 2048–2053 (2011).
13. F. Marsili, F. Najafi, E. Dauler, R. J. Molnar, and K. K. Berggren, "Afterpulsing and instability in superconducting nanowire avalanche photodetectors," Appl. Phys. Lett. **100**(11), 112601 (2012).

14. R. Cristiano, M. Ejrnaes, A. Casaburi, S. Pagano, F. Mattioli, A. Gaggero, and R. Leoni, "Superconducting single photon detectors based on multiple cascade switches of parallel NbN nanowires," in *Proc. SPIE 8072, Photon Counting Applications, Quantum Optics, and Quantum Information Transfer and Processing III,* I. Prochazka and J. Fiurásek, eds. (2011), Vol. 8072, p. 807205.
15. J. K. W. Yang, A. J. Kerman, E. A. Dauler, V. Anant, K. M. Rosfjord, and K. K. Berggren, "Modeling the Electrical and Thermal Response of Superconducting Nanowire Single-Photon Detectors," IEEE Trans. Appl. Supercond. **17**(2), 581–585 (2007).
16. A. J. Kerman, J. K. W. Yang, R. J. Molnar, E. A. Dauler, and K. K. Berggren, "Electrothermal feedback in superconducting nanowire single-photon detectors," Phys. Rev. B **79**(10), 100509 (2009).
17. Q. Zhao, T. Jia, M. Gu, C. Wan, L. Zhang, W. Xu, L. Kang, J. Chen, and P. Wu, "Counting rate enhancements in superconducting nanowire single-photon detectors with improved readout circuits," Opt. Lett. **39**(7), 1869–1872 (2014).
18. A. J. Kerman, D. Rosenberg, R. J. Molnar, and E. A. Dauler, "Readout of superconducting nanowire single-photon detectors at high count rates," J. Appl. Phys. **113**(14), 144511 (2013).
19. F. Najafi, F. Marsili, E. A. Dauler, R. J. Molnar, and K. K. Berggren, "Timing performance of 30-nm-wide superconducting nanowire avalanche photodetectors," Appl. Phys. Lett. **100**(15), 152602 (2012).

1. Introduction

Superconducting nanowire single-photon detectors (SNSPDs) are of great interest in fields such as quantum information processing, linear-optics quantum computation [1], and quantum communication [2] due to the high efficiency, low dark counts, fast recovery time, and low timing jitter [3]. However, one of the limiting factors in their applications is the small amplitude of output pulses, which are on the order of a millivolt. The presence of noise in the readout system can overwhelm these small pulses, and so amplification of the pulse is necessary for accurate readout. For a standard SNSPD architecture of a single nanowire, additional timing jitter [4,5] and dark counts typically result from electric noise if the signal-to-noise ratio (SNR) of its output pulses is low. While external amplifiers can be used to achieve amplification, they ultimately add noise and reduce the SNR of the readout. Spatially multiplexing superconducting nanowire single-photon detectors can realize a single-photon array or a photon-number resolving (PNR) detector [6–8]. However, a scalable readout circuit has not yet been realized. Recently, analogous readout architectures which integrated passive electronics with multiple SNSPDs were reported [9,10], using a basic idea of encoding information of photon position or photon number on pulse amplitude. But, scaling up the array or PNR detector was limited by the SNR of a single element which was a typical SNSPD.

Increasing the amplitude of a detector's output pulse is a direct way to increase SNR, therefore, superconducting nanowire avalanche photodetectors (n-SNAPs, also named cascade-switching superconducting single-photon detectors) [11,12] were developed. The n-SNAP is a variation of the SNSPD, with n individual detection nanowires in parallel instead of a single, longer, detection nanowire. The parallelized SNAP architecture increases the total amount of current that the detector carries, and as a result increases the amplitude of output pulses. A typical n-SNAP implementation is shown in Fig. 1(a) and an equivalent circuit of a detection nanowire is shown in Fig. 1(b). In an n-SNAP, a single photon absorbed in one detection nanowire creates a resistive hotspot, expelling current from that nanowire and redistributing it into to the n-1 neighboring detection nanowires. If the n-SNAP is biased with enough current, the redistributed current will cause an avalanche in the neighboring nanowires. During this avalanche, the current added to each neighboring nanowire causes it to exceed its critical current (I_{CN}), initiating an avalanche of resistive hotspots. Once all the detection nanowires are resistive, the current from all n nanowires is diverted into the output, and so an n-SNAP can generate output pulses n times larger than pulses of an SNSPD. Additionally, since this process occurs at the device level, the amplification mechanism does not add external noise and so the SNR scales proportionally with n as well. Unfortunately, the n-SNAP design has not scaled well for $n > 4$ detection nanowires [12]. As n is increased, the portion of current that each of the n-1 neighboring nanowires receives from the redistributed current shrinks. For an n-SNAP biased at I_B with a critical current I_C, the bias condition

necessary to guarantee an avalanche of all the detection nanowires into a resistive state is $I_B \geq I_C(N-1)N$. The minimal I_B that initiates an avalanche is defined as the avalanche current (I_{AV}). As n increases, I_{AV} rapidly approaches I_C, which can cause problems such as afterpulsing, latching, and increased dark counts [13].

2. Design and fabrication

Here, we introduce a modified n-SNAP design, which we refer to as n-*SNAP. The n-*SNAP uses multiple avalanche stages to increase the total number of nanowires beyond four while maintaining a low avalanche current. Using inductors arranged in a binary-tree layout, we can control the evolution of avalanche such that the redistributed current from the initial triggered nanowire only needs to overbias one neighboring nanowire at first, but will still cause a resistive avalanche across the whole device. The idea of using multiple parallel SNSPDs was also reported in [14] as a way to increase the active area of a detector. However, in our design, configuration of the nanowires and inductor network is a binary-tree format used specifically to generate a controlled avalanche and increase n.
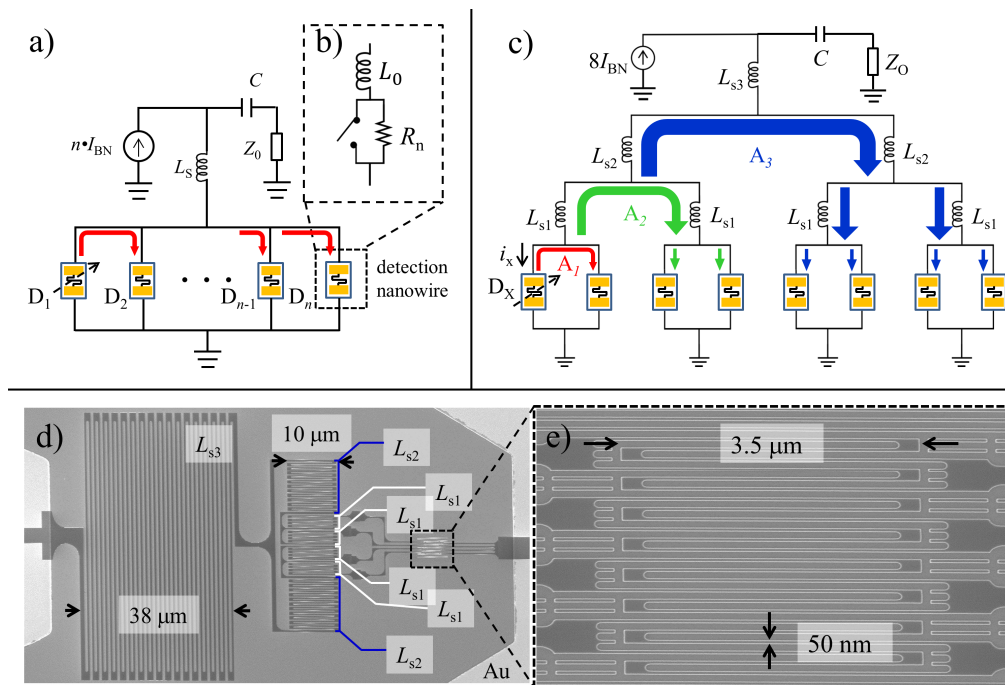

Fig. 1. (a) Schematic diagram of an n-SNAP in conventional avalanche architecture. Nanowires from D_1 to D_n are paralleled directly. A choke inductor (L_S) is connected in series to block the current to leak to the load. (b) Equivalent circuit of a detection nanowire. L_0 is the kinetic inductance of the nanowire. R_n is the time-varying resistance when the switch is open by a photon detection. (c) Schematic diagram of an 8-*SNAP. D_x and i_x represent the xth individual nanowire and the current passing through it, respectively. The colored arrows show the successive avalanches A_1 (red), A_2 (green) and A_3 (blue) when D_1 (leftmost detection nanowire) is triggered. (d) SEM images of an 8-*SNAP. The whole device is labeled according to the corresponding circuit parts shown in (c). (e) A close-up of the photon-sensitive individual nanowires, consisting of eight 50 nm wide nanowires.

The schematic diagram of the 8-*SNAP is shown in Fig. 1(c) and the SEM pictures of a fabricated device are shown in Figs. 1(d) and (e). In the 8-*SNAP, the eight detection nanowires were arranged to form four pairs, such as D_1 and D_2. Each pair was connected through a binary tree of choke inductors to form secondary and tertiary avalanches. To

control the avalanche sequence, the inductors are designed such that $L_{S3} > L_{S2} > L_{S1} \gg L_0$, where L_0 is the inductance of one detection nanowire. For our niobium nitride film, the inductance is about 80 pH/square. The estimated inductances were L_{S3} = 341 nH, L_{S2} = 70 nH, L_{S1} = 40 nH, and L_0 = 17 nH. The arrows in Fig. 1(c) illustrate the order in which the avalanches occur when the detection nanowire D_1 is triggered. Current is diverted from D_1 and flows into the adjacent nanowire D_2, because the choke inductance L_{S1} acts as a high-impedance barrier to the other possible current paths at these short timescales. When i_2, the current through D_2, exceeds I_{CN}, D_2 is triggered to resistive state. At this point, both D_1 and D_2 are resistive, and because we have designed L_{S2} to be larger than L_{S1}, most of the current diverted from the D_1/D_2 2-SNAP is routed to the D_3/D_4 2-SNAP through the lowest-impedance path L_{S1}. As long as i_3 and i_4 exceed I_{CN}, the second avalanche A_2 follows. A similar process then cascades to the four remaining detection nanowires, creating the third avalanche A_3. When all the nanowires have switched to the resistive state, the bias current is forced into the external load Z_0, generating a voltage pulse for detection.

We simulated the circuit using an electrothermal model and calculated the evolution of current in each nanowire [15]. After D_1 was triggered, the other nanowires were observed to go to resistive in the expected order. The current distribution in each nanowire, as shown in Fig. 2(a), depicts the sequence of the avalanches. Although the current in each nanowire varied during the avalanches, due to the electrothermal feedback in the nanowire [15,16], all of the currents eventually converged and evolved identically after the final avalanche A_3 (~40 ps after D_1 was triggered).

We designed, fabricated and characterized 8-*SNAPs and also fabricated 2-SNAPs, 3-SNAPs and SNSPDs for comparison. All detectors were made from ultrathin niobium nitride (NbN) film on a single MgO substrate. The critical temperature of the film was 11.4 K and the sheet resistance was 429 Ω/square. Detectors were measured in a probe station at a sample temperature of 2.4 K. The critical current, width, pitch and active area of these devices are: 8-*SNAP (65.0 µA, 50nm, 150nm, 3.5 × 3.5 µm^2), 2-SNAP (15.5 µA, 50nm, 150nm, 3.5 × 1.4 µm^2), 3-SNAP (24.0 µA, 50nm, 150nm, 3.5 × 2.2 µm^2), and 50 nm wide SNSPD (7.2 µA, 50nm, 150nm, 3.5 × 2.8 µm^2). A mode-locked laser at a wavelength of 1.5 µm with sub-picosecond pulse width and 77 MHz repetition rate was used as the light source in measuring detection efficiency and timing jitter.

3. Characterization

As one important motivation of our successive-avalanche architecture, the avalanche current of n-*SNAP was expected to be lower than the avalanche current of an n-SNAP, therefore, giving more bias margin for paralleling more nanowires to achieve higher signal amplification. As we have discussed, it is difficult to fabricate a well functional n-SNAP with $n > 4$, but we were nevertheless able to compare the architectures by using idealized devices in an electrothermal simulation. We ran the simulation several times, varying the bias current in the detection nanowire (I_{BN}). Figure 2(b) shows the output pulses from simulations of an 8-*SNAP with the bias current normalized to the critical current (I_{BN}/I_{CN}) set to 0.70, 0.75, and 0.80. The pulses had three levels, which corresponded to the cases where A_1, A_2 or A_3 was the final avalanche. When the normalized bias current was at or below 0.65, even the pair of D_1 and D_2 was not triggered. By sweeping the normalized current from 0.75 to 0.80, we determined the lowest bias current which was able to trigger the third avalanche. This lowest bias current of each nanowire, multiplied by a factor of eight, was the minimum avalanche current for the 8-*SNAP and had a value of I_{AV_S} = 0.78I_{C8}, where I_{C8} = 8I_{CN} was the total critical current of the eight nanowires. For simulating the avalanche current of the 8-SNAP (I_{AV_C}) with the same critical current, its choke inductor L_s was set to the same inductance as L_{S3} in an 8-*SNAP. Applying the same simulation method, we found I_{AV_C} = 0.91I_{C8}. Comparing these simulation results, the normalized avalanche current of 8-*SNAP was 13%

lower than the normalized avalanche current of 8-SNAP, showing that the successive-avalanche facilitated the avalanche to happen at low bias current.

To verify the fabricated 8-*SNAP operating in a full avalanche regime, we experimentally measured the avalanche current (I_{AV_E}). The detectors were measured in a probe station and flood illuminated by a single-mode fiber. We calculated the number of incident photons on the detector by measuring the distance between the fiber tip and the chip, and characterizing the fiber's numerical aperture. Consequently, the device detection efficiency (DDE) was the ratio of the rate of detection pulses to the rate of incident photons. When the device is biased above its avalanche current, the measured detection efficiency is independent to the incident photon flux, since a single photon absorption can produce a full avalanche. Thus, from measuring DDE versus the bias current at different incident photon fluxes, we can deduce I_{AV_E} as the lowest bias current where the curves for various photon fluxes overlap. As shown in Fig. 2(c), this value was $I_{AV\_E} = 0.78I_{C8}$, in agreement with the value from our electrothermal simulation. Additionally, we corroborated this measurement by comparing the DDE of the 8-*SNAP to a standard, single-nanowire, 50 nm wide SNSPD. Above the normalized bias current of 0.78, the DDE curves of the 8-*SNAP overlapped with the curve of the SNSPD as expected from single photon detections in identical nanowires. Because of the low avalanche current, the nanowires in the 8-*SNAP could be biased lower, producing fewer dark counts. In other words, this low avalanche current provides a wide bias margin for optimizing the detection performance, especially for detectors with saturated DDE. In the 8-*SNAP, the DDE did not saturate due to fabrication defects in the 50 nm wide nanowires. By optimizing the fabrication process or reducing the width of the nanowires, a saturated efficiency should be expected.

Ideally, the avalanche current of an 8-*SNAP would be approximately equal to a 2-SNAP. This equivalence should exist because at the first avalanche stage, such as at A_1, the current expelled from a detection nanowire only needs to over-bias one neighbor, similar to the two-parallel-nanowire setup in a 2-SNAP. We measured the 2-SNAP and 3-SNAP, finding their experimental avalanche currents of $I_{AV\_2E} = 0.72I_{C2}$ and $I_{AV\_3E} = 0.79I_{C3}$, where I_{C2} and I_{C3} are the critical currents for the 2-SNAP and 3-SNAP, respectively. According to these values, the normalized avalanche current I_{AV_E}/I_{C8} of the 8-*SNAP was higher than I_{AV_2E}/I_{C2} of the 2-SNAP and closer to I_{AV_3E}/I_{C3} of the 3-SNAP, which is slightly different to an ideal equivalence because of the leakage currents in each avalanche stage.
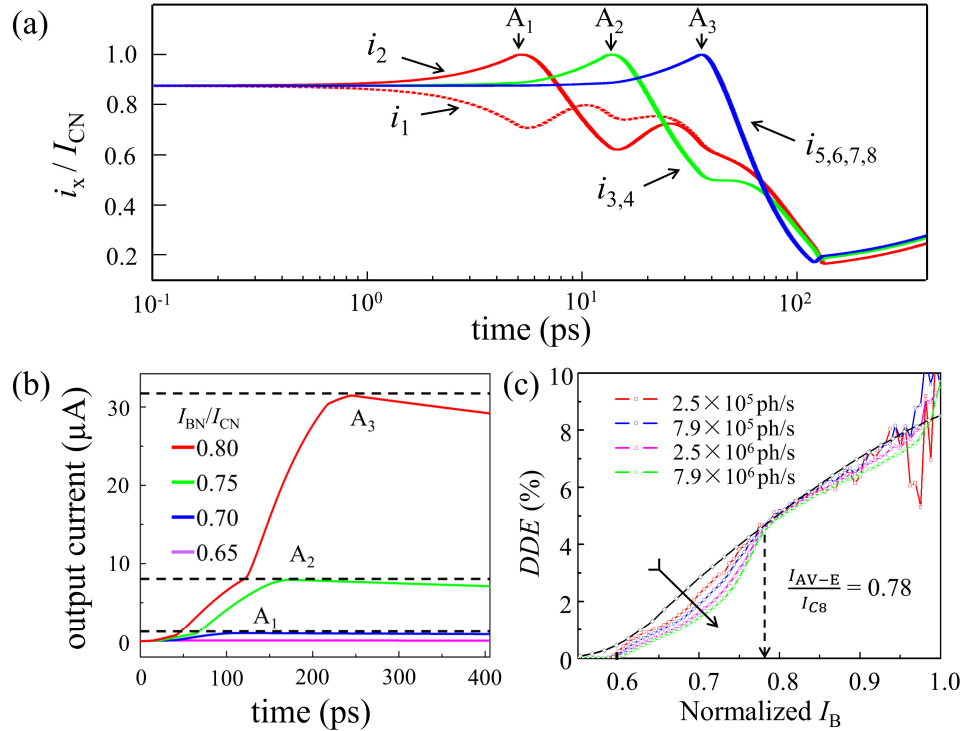
Fig. 2. (a) Electrothermal simulation of the normalized currents through the eight nanowires in an 8-*SNAP. When the current passing through the nanowire exceeds I_{CN}, the avalanche processes are triggered, denoted as A_1, A_2 and A_3. (b) Electrothermal simulation of the output pulses at I_{BN} of $0.80I_{CN}$ (red), $0.75I_{CN}$ (green), $0.70I_{CN}$ (blue) and $0.65I_{CN}$ (purple). The dashed lines show the levels of the output current corresponding to the cases that the last avalanche is A_1, A_2 and A_3. (c) *DDE* vs normalized I_B for the SNSPD (black) and the 8-*SNAP illuminated at different incident photon fluxes as shown in the legend. As the photon flux increases, depicted by the arrow, the *DDE* curves of the 8-*SNAP shift away from the *DDE* curve of the SNSPD. The dashed arrow shows the inflection point of the *DDE* curves, which is $0.78I_{C8}$ and is the experimental avalanche current of the 8-*SNAP, I_{AV_E}. Curves measured under low incident photon fluxes are noisy when I_B is close to the critical current, because the photon detection count rate is lower than the dark count rate, resulting in high background noise.

To demonstrate the eight-fold signal amplification of the 8-*SNAP versus a standard SNSPD in the same width of 50 nm, we measured single-shot pulse traces of the 8-*SNAP and SNSPD. The traces are shown in Fig. 3(a). The critical current of the 50 nm wide SNSPD was 7.2 μA and the critical current of the 8-*SNAP was 65 μA. We biased both devices at 83% of their critical currents. The peak values of the 8-*SNAP pulse and the SNSPD pulse were 109.1 mV and 13.5 mV, respectively. This corresponded to an eight-fold enhancement of the signal, proportional to *n* = 8 as expected. This proportionality also shows that the pulse of the 8-*SNAP was the result of a full avalanche sequence containing all the current from all of the detection nanowires, and the successive avalanches worked. Considering the ~100 ns long duration of the 8-*SNAP's output pulse, the system readout noise (peak-to-peak value) was extracted in a 100 ns long time window from the acquired traces before the pulses arrive. The noise was 7.9 mV for the 8-*SNAP and it was 7.3 mV for the SNSPD, which were almost identical and were dominated by the amplifier noise. Therefore, the *SNR* of the 8-*SNAP (109.1/7.9 = 13.8) was also increased by a factor of 8 over the *SNR* of the SNSPD (13.5/7.3 = 1.8). The large *SNR* pulses were easily discriminated from the background noise even with a highly lossy RF cable connection. This could be useful in arrays of SNSPDs

which use large numbers of coax lines for readout, since those lines are typically highly lossy in order to maintain a low thermal conductivity (due to the Wiedemann-Franz law).

As shown by the pulse traces in Fig. 3(a), the falling edge of the 8-*SNAP pulse showed an overshoot as the pulse returns to zero; this was due to the low frequency cutoff of the amplifiers. This overshoot indicates a large kinetic inductance of the device which is mainly due to the choke inductors. Reducing the choke inductance could reduce the reset time of the 8-*SNAP, but it also prevents the avalanche formation because the current from the triggered nanowire leaks more easily to the load instead of injecting into the neighboring nanowires, resulting in an increase of the avalanche current [13]. In the measured circuit, the recovery time constant is set by L_T/Z_0, where $L_T \approx L_{S3}$ is the total kinetic inductance of the device and Z_0 = 50 Ω is the load resistance that the output pulses apply on. In the measured 8-*SNAP, because of the large inductance from the inductor binary tree, the recovery time is slowed down. However, in an optimized circuit, the 8-*SNAP speed should only be limited by the time of cooling down hotspot and the readout circuits just like an SNSPD [17,18], with a small speed reduction accounted for the delay caused by avalanche latency. For example, adding a series resistor R_S close to the device, can reduce the time constant to $L_T/(R_S + Z_0)$ and thus can speed up the current recovery in the 8-*SNAP [15]. There was no afterpulsing in the 8-*SNAP as long as it was not biased very close to the critical current. The bias condition with no afterpulsing existed because the avalanche current of 8-*SNAP was low, showing another advantage of our multiple-avalanche architecture.
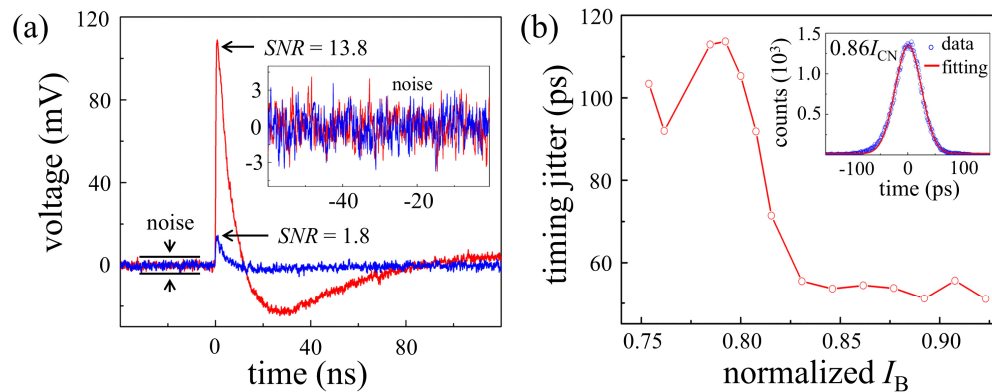

Fig. 3. (a) Traces of a single pulse from the 8-*SNAP (red) and the SNSPD (blue). The signal is extracted from the peak value of the average pulses (not shown here) and the peak-to-peak noise is taken from the traces before the pulses arrive in a time window of 100 ns. The inset figure shows the noise floor of our 8-*SNAP is nearly identical to the noise floor of the SNSPD. (b) Timing jitter versus normalized I_B. The inset figure shows the jitter performance at $0.86I_{C8}$. The delay distribution is fitted to a Gaussian profile.

Since the dynamic processes of the nanowires in an n-SNAP are more complex than a SNSPD with single nanowire, we measured the timing jitter of the 8-*SNAP to show that the successive-avalanche architecture does not add significant timing jitter. The timing jitter was extracted by analyzing the variance in time-delay between the synchronized pulses from a fast photodiode and the output pulses from the detector [19]. The trigger level was set to a half of the pulse amplitude. The jitter was measured for several values of I_B, and the results are shown in Fig. 3(b). Similar to n-SNAPs in conventional architecture, the histogram of the time delay appeared to be asymmetric and showed multiple peaks below the avalanche current [19]. However, when the device was biased above the avalanche current, the histogram of the delay has a roughly Gaussian profile as shown in the Fig. 3(b) inset. The value of the timing jitter was extracted from the full-width-at-half-maximum (FWHM) of the histogram of the time delay. For the 8-*SNAP, the jitter had a minimum plateau of ~54 ps,

showing negligible dependence on the bias current above 0.82 I_{C8} in the absence of additional timing jitter from voltage noise [4,5]. A precise jitter measurement cannot be taken for the 50 nm wide SNSPD because of its SNR was too low. The jitter was 46 ps for the 2-SNAP biased at 13 µA and it was 53 ps for the 3-SNAP biased at 22 µA. Therefore, the timing jitter of the 8-*SNAP was similar to a 2-SNAP and a 3-SNAP, showing the successive-avalanche architecture didn't give additional timing jitter compared to the conventional design.

4. Conclusion

In conclusion, we have demonstrated a parallel SNSPD architecture with successive avalanches. The architecture consisted of detection nanowires and choke inductors arranged in a binary-tree layout. For the demonstrated 8-*SNAP, the output signal and the SNR of the output pulse were measured to be eight times higher than the equivalent SNSPD of the same nanowire width. The normalized avalanche current was measured to be 0.78, which was 13% lower than the ideal normalized avalanche current of an equivalent 8-SNAP using conventional design. The detector had a minimum timing jitter of 54 ps, which was independent of the normalized bias current above 0.82, showing that the successive-avalanche architecture didn't deteriorate the timing performance. The binary-tree design can be easily scaled to use more nanowires in parallel, in order to generate even greater amplification. However, the inductor network needs to be optimized to speed up the current recovery time of the nanowires, for example, by connecting a series resistor to reduce the current recovery time. The high SNR, low timing jitter, and monolithic integration suggest that this architecture is promising for applications that require larger pulse amplitudes, such as single-photon arrays, photon-number-resolving detectors, or feed-forward on-chip logic for integrated photonic quantum-information processing.